

Channel Estimation for mmWave MIMO using sub-6 GHz Out-of-Band Information

Faruk Pasic*, Markus Hofer[‡], Mariam Mussbah*[†], Sebastian Caban*, Stefan Schwarz*, Thomas Zemen[‡] and Christoph F. Mecklenbräuker*

*Institute of Telecommunications, TU Wien, Vienna, Austria

[†]Christian Doppler Laboratory for Digital Twin assisted AI for sustainable Radio Access Networks

[‡]AIT Austrian Institute of Technology, Vienna, Austria

faruk.pasic@tuwien.ac.at

Abstract—Future wireless multiple-input multiple-output (MIMO) communication systems will employ sub-6 GHz and millimeter wave (mmWave) frequency bands working cooperatively. Establishing a MIMO communication link usually relies on estimating channel state information (CSI) which is difficult to acquire at mmWave frequencies due to a low signal-to-noise ratio (SNR). In this paper, we propose three novel methods to estimate mmWave MIMO channels using out-of-band information obtained from the sub-6 GHz band. We compare the proposed channel estimation methods with a conventional one utilizing only in-band information. Simulation results show that the proposed methods outperform the conventional mmWave channel estimation method in terms of achievable spectral efficiency, especially at low SNR and high K-factor.

Index Terms—channel estimation, mmWave, sub-6 GHz, 5G, MIMO, out-of-band information, beamforming.

I. INTRODUCTION

Today's wireless communication systems operate mainly in the sub-6 GHz frequency bands. Due to the spectrum shortage, sub-6 GHz bands can not keep up with the growing demand for high data rates. Fortunately, significantly more bandwidth is available in millimeter wave (mmWave) bands (10 GHz – 300 GHz), which enables high data rate transmissions [1]. To provide a sufficient link margin, in most mmWave systems, antenna arrays will be used at the transmitter and receiver side. This creates many opportunities to apply multiple-input multiple-output (MIMO) communication techniques such as directional beamforming [2]. Therefore, mmWave MIMO communication is a promising technology for next-generation wireless systems [3].

Configuring mmWave antenna arrays is challenging. The main challenge in using mmWave frequency bands is link establishment, which is done by designing the precoder and combiner [4]. The precoder and combiner design usually relies on channel state information (CSI), which is difficult to acquire at mmWave frequencies due to low pre-beamforming signal-to-noise ratio (SNR). Hence, the performance of CSI estimation is directly related to the coverage capability of wireless systems, which is the main obstacle of fifth generation (5G) and beyond systems employing mmWave bands.

Many multi-band measurement campaigns in different environments have shown that mmWave frequency bands have similar propagation characteristics as sub-6 GHz bands [5]–[10]. Specifically, the multipath components were found to be similarly distributed in these two frequency bands. Since mmWave systems will likely be deployed in conjunction with sub-6 GHz systems [11], the opportunity arises to use these two bands cooperatively to achieve a better system throughput.

So far, several beam-selection strategies to leverage sub-6 GHz out-of-band information as side information on mmWave band have been proposed. In [12], the authors propose using spatial information extracted at sub-6 GHz to improve mmWave compressed beam selection. Furthermore, two approaches (non-parametric and parametric) to translate the lower frequency spatial correlation to the higher frequency have been proposed in [13]. In [14], the authors analyze the feasibility of using low-band channel information for coarse estimation of high-band beam directions. The authors in [15], [16] propose a deep learning-based beam selection algorithm for mmWave bands, exploiting sub-6 GHz channel information. However, the idea of exploiting sub-6 GHz out-of-band information for mmWave channel estimation has not been investigated yet.

Contribution: In this paper, we propose three novel pilot-aided channel estimation methods for mmWave MIMO systems based on out-of-band information. We exploit the relationship between line-of-sight (LOS) channel components across different frequency bands and estimate the mmWave channel with the aid of adapted channel coefficients obtained in the sub-6 GHz band. We evaluate the proposed methods through simulations in terms of spectral efficiency (SE).

Organization: In Section II, we present the system model considered in this work. Section III presents the proposed channel estimation methods. The performance comparison is given in Section IV. Finally, Section V concludes the paper.

Notation: Bold uppercase letters \mathbf{X} denote matrices and bold lowercase letters \mathbf{x} denote vectors. We use the superscript $(\cdot)^H$ for Hermitian transposition and the superscript $(\cdot)^{(b)}$ for frequency-band dependent values, where $b \in \{s, m\}$. Here, s denotes the sub-6 GHz frequency band and m denotes the mmWave frequency band. Operation \odot represents element-wise multiplication and $\|\cdot\|_F$ denotes the Frobenius norm.

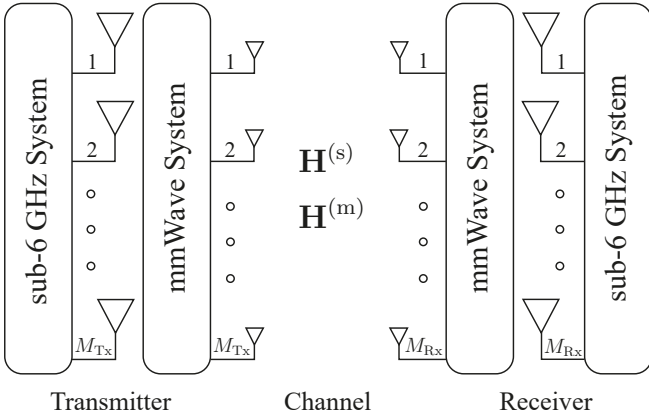


Fig. 1. A multi-band MIMO transmission system with co-located sub-6 GHz and mmWave antenna arrays. $\mathbf{H}^{(s)}$ denotes the sub-6 GHz MIMO channel. $\mathbf{H}^{(m)}$ denotes the mmWave MIMO channel.

II. SYSTEM MODEL

We consider a point-to-point multi-band MIMO system, where sub-6 GHz and mmWave systems operate simultaneously. The transmitter consists of M_{Tx} sub-6 GHz and M_{Tx} mmWave antenna elements, while the receiver is equipped with an antenna array comprising M_{Rx} sub-6 GHz and M_{Rx} mmWave antenna elements. The sub-6 GHz and mmWave parts of the system are arranged as a uniform linear array (ULA) of dipole antennas, modeled as isotropic point sources (see Fig. 1). We assume that the sub-6 GHz and mmWave antenna arrays are co-located and aligned. Both arrays have the same number of antenna elements mutually separated by $0.5\lambda^{(m)}$, where $\lambda^{(m)}$ represents the wavelength of the mmWave system. The small antenna spacing for the sub-6 GHz array can be achieved by a compact design, as proposed in [17]. Furthermore, we assume perfect time and frequency synchronization at the receiver. The transmitter and receiver are equipped with one radio frequency (RF) chain per antenna, thereby allowing for fully digital beamforming for both sub-6 GHz and mmWave systems [18].

We consider an orthogonal frequency-division multiplexing (OFDM) system with $N^{(b)}$ subcarriers. Blocks of $N^{(b)}$ symbols modulated by quadrature amplitude modulation (QAM) are mapped onto $N^{(b)}$ different subcarriers to construct OFDM symbols. The OFDM system converts a broadband frequency-selective channel into narrowband frequency flat channels with the help of a discrete Fourier transform (DFT) and application of a cyclic prefix [19], [20]. The channel at the OFDM subcarrier n is described by an $M_{\text{Rx}} \times M_{\text{Tx}}$ dimensional complex-valued channel matrix $\mathbf{H}^{(b)}[n]$, employing the equivalent complex baseband representation of the OFDM system.

A. Channel Model

We consider a frequency-selective Rician fading channel model defined as

$$\mathbf{H}^{(b)}[n] = \sqrt{\eta^{(b)}} \left(A_{\text{fs}}^{(b)} \mathbf{H}_{\text{fs}}^{(b)}[n] + A_{\text{rp}}^{(b)} \mathbf{H}_{\text{rp}}^{(b)}[n] \right) \quad (1)$$

where $\eta^{(b)}$ is the path loss coefficient, $A_{\text{fs}}^{(b)} = \sqrt{K^{(b)} / (1 + K^{(b)})}$ denotes the free-space scaling factor, $A_{\text{rp}}^{(b)} = \sqrt{1 / (1 + K^{(b)})}$ represents the Rayleigh-part scaling factor and $K^{(b)}$ denotes the Rician K -factor. Based on the measurements presented in [21], due to the less pronounced multipath components at mmWave bands compared to sub-6 GHz bands, we assume that the mmWave K -factor $K^{(m)} = 10K^{(s)}$. The deterministic free-space channel $\mathbf{H}_{\text{fs}}^{(b)}[n]$ is defined by

$$\mathbf{H}_{\text{fs}}^{(b)}[n] = e^{-j\frac{2\pi}{\lambda^{(b)}}\mathbf{D}}, \quad (2)$$

where

$$\mathbf{D} = \begin{bmatrix} d_{1,1} & \cdots & d_{1,M_{\text{Tx}}} \\ \vdots & \ddots & \vdots \\ d_{M_{\text{Rx}},1} & \cdots & d_{M_{\text{Rx}},M_{\text{Tx}}} \end{bmatrix} \in \mathbb{R}^{M_{\text{Rx}} \times M_{\text{Tx}}} \quad (3)$$

represents the distances between specific transmit and receive antenna elements and $\lambda^{(b)}$ denotes the wavelength. The Rayleigh channel matrix $\mathbf{H}_{\text{rp}}^{(b)}[n]$ consists of independent complex Gaussian random variables with the power of one.

The path loss coefficient for mmWave bands is defined by

$$\eta^{(m)} = \left(\frac{4\pi d f_c^{(m)}}{c_0} \right)^2 = \left(\frac{4\pi d \sqrt{\alpha} f_c^{(s)}}{c_0} \right)^2 = \alpha \eta^{(s)}, \quad (4)$$

where d denotes the distance between the transmitter and the receiver, c_0 is the speed of light, $\eta^{(s)}$ represents the free space path loss for the sub-6 GHz band and $\sqrt{\alpha} = f_c^{(m)} / f_c^{(s)}$ denotes the carrier frequency ratio between the sub-6 GHz band and the mmWave band. Furthermore, we assume the same transmit power P_{T} for both frequency bands. Since mmWave systems tend to use larger bandwidth and can have a noise figure different to sub-6 GHz systems, we introduce $\beta = \frac{B^{(m)} F^{(m)}}{B^{(s)} F^{(s)}}$ as the ratio of sub-6 GHz and mmWave bandwidths and noise figures. Then, the obtained pre-beamforming mmWave SNR for the single receive antenna element can be expressed by

$$\begin{aligned} \gamma^{(m)} &= \frac{P_{\text{T}}}{\eta^{(m)} k_{\text{B}} T B^{(m)} F^{(m)}} = \frac{P_{\text{T}}}{\alpha \eta^{(s)} k_{\text{B}} T \beta B^{(s)} F^{(s)}} \\ &= \gamma^{(s)} \frac{1}{\alpha \beta}, \end{aligned} \quad (5)$$

where k_{B} represents the Boltzmann constant and T denotes the receiver temperature. A sub-6 GHz system with $\alpha\beta$ times higher SNR has benefits. These benefits will be highlighted below.

B. Link Establishment

Establishing a communication link consists of a training phase and data transmission. The wireless channel is estimated at sub-6 GHz and mmWave frequency bands during the training phase. The channel estimates obtained at the sub-6 GHz and mmWave bands are then utilized for data transmission at the mmWave band. We do not transmit data in the sub-6 GHz band.

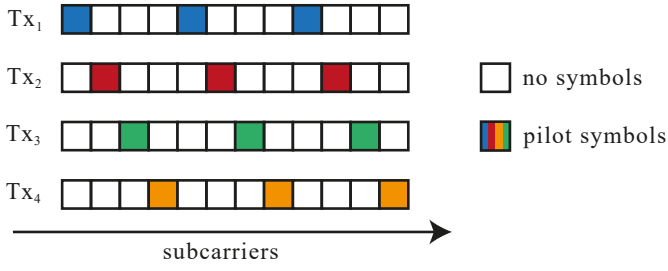


Fig. 2. Pilot symbols at each antenna occupy a certain number of subcarriers such that they do not overlap in the frequency domain.

1) *Training Phase*: During the training phase, each transmit antenna is assigned pilot symbols that are known at the receiver. The pilot symbols $\phi^{(b)}[n] \in \mathbb{C}^{M_{\text{Tx}} \times 1}$ generated from the QAM alphabet are distributed over $N^{(b)}$ subcarriers so that each antenna occupies a certain number of non-overlapping subcarriers. The pilot allocation at the t -th transmit antenna is given by

$$\phi_t^{(b)}[n] = \begin{cases} \phi^{(b)}[n], & n \in \{t, t + M_{\text{Tx}}, \dots, N^{(b)}\} \\ 0, & \text{else} \end{cases} \quad (6)$$

A pilot allocation example for $M_{\text{Tx}} = 4$ transmit antennas is shown in Fig. 2. The input-output relationship for the training phase is given by

$$\mathbf{y}^{(b)}[n] = \mathbf{H}^{(b)}[n]\phi^{(b)}[n] + \mathbf{w}^{(b)}[n], \quad (7)$$

where the received signal is denoted by $\mathbf{y}^{(b)}[n] \in \mathbb{C}^{M_{\text{Rx}} \times 1}$ and the additive white Gaussian noise (AWGN) added at the receiver with the power of σ_w^2 is denoted by $\mathbf{w}^{(b)}[n] \in \mathcal{CN}(0, \sigma_w^2 \mathbf{I}_{M_{\text{Rx}}})$. At the receiver, the least-square (LS) estimates of the channel are obtained at pilot positions $n_t \in \{t, t + M_{\text{Tx}}, \dots, N^{(b)}\}$. Further, linear interpolation is performed to estimate the channel at non-occupied subcarrier positions, resulting in an estimated channel $\tilde{\mathbf{H}}^{(b)}[n] \in \mathbb{C}^{M_{\text{Rx}} \times M_{\text{Tx}}}$. Since the channel is estimated at the receiver, the CSI has to be fed back to help the transmitter select the best beamforming matrix. Therefore, the estimated channel $\tilde{\mathbf{H}}^{(b)}[n] \in \mathbb{C}^{M_{\text{Rx}} \times M_{\text{Tx}}}$ is sent to the transmitter, assuming perfect feedback. Furthermore, we assume here that the channel in (1) stays relatively stable over time (long coherence time), so the channel estimation and sending the estimated channel to the transmitter via feedback is only performed infrequently.

2) *Data Transmission*: For the data transmission phase, we consider only the mmWave system. The estimated channels $\tilde{\mathbf{H}}^{(s)}[n]$ and $\tilde{\mathbf{H}}^{(m)}[n]$ are processed using the three methods proposed in Section III. The resulting mmWave channel estimate $\bar{\mathbf{H}}^{(m)}[n]$ is then utilized for achieving the highest performance of the MIMO channel by singular value decomposition (SVD) based unitary precoding and combining. The compact-form SVD of the channel matrix $\bar{\mathbf{H}}^{(m)}[n]$ can be written as

$$\bar{\mathbf{H}}^{(m)}[n] = \bar{\mathbf{Q}}^{(m)}[n] \bar{\Sigma}^{(m)}[n] \left(\bar{\mathbf{F}}^{(m)}[n] \left(\mathbf{P}^{(m)} \right)^{1/2} \right)^{\text{H}}, \quad (8)$$

where the semi-unitary matrix $\bar{\mathbf{Q}}^{(m)}[n] \in \mathbb{C}^{M_{\text{Rx}} \times \ell_{\text{max}}}$ denotes the matrix of left singular vectors and $\bar{\mathbf{F}}^{(m)}[n] \in \mathbb{C}^{M_{\text{Tx}} \times \ell_{\text{max}}}$ represents the matrix of right singular vectors. The singular value matrix is given by

$$\bar{\Sigma}^{(m)}[n] = \text{diag} \left(\bar{\sigma}_{(1)}^{(m)}[n], \dots, \bar{\sigma}_{(\ell_{\text{max}})}^{(m)}[n] \right), \quad (9)$$

where the i -th diagonal element $\bar{\sigma}_{(i)}^{(m)}[n]$ of the singular value matrix is equals the i -th largest singular value of $\bar{\mathbf{H}}^{(m)}[n]$. Assuming a full-rank channel, the maximum number of streams is $\ell_{\text{max}} = \min(M_{\text{Rx}}, M_{\text{Tx}})$. The power loading matrix is given by

$$\mathbf{P}^{(m)} = \text{diag} \left(p_{(1)}^{(m)}, \dots, p_{(\ell_{\text{max}})}^{(m)} \right), \quad (10)$$

where $p_{(1)}^{(m)} = p_{(2)}^{(m)} = \dots = p_{(\ell_{\text{max}})}^{(m)} = P_{\text{T}}/\ell_{\text{max}} > 0$ and the total transmit power constraint

$$\left\| \bar{\mathbf{F}}^{(m)}[n] \left(\mathbf{P}^{(m)} \right)^{1/2} \right\|_F^2 = P_{\text{T}} \quad (11)$$

is satisfied by the precoder.

The symbol vector to be transmitted is written as $\mathbf{x}^{(m)}[n] \in \mathbb{C}^{M_{\text{Tx}} \times 1}$. Prior to transmission over the wireless channel, the symbol vector $\mathbf{x}^{(m)}[n]$ is precoded with a precoding matrix $\bar{\mathbf{F}}^{(m)}[n]$. At the receiver, combining is performed with a combining matrix $\bar{\mathbf{Q}}^{(m)}[n]$. With this notation, the input-output relationship for the data transmission phase is then given by

$$\mathbf{y}^{(m)}[n] = \left(\bar{\mathbf{Q}}^{(m)}[n] \right)^{\text{H}} \mathbf{H}^{(m)}[n] \left(\mathbf{P}^{(m)} \right)^{1/2} \bar{\mathbf{F}}^{(m)}[n] \mathbf{x}^{(m)}[n] + \left(\bar{\mathbf{Q}}^{(m)}[n] \right)^{\text{H}} \mathbf{w}^{(m)}[n], \quad (12)$$

where the received signal is denoted by $\mathbf{y}^{(m)}[n] \in \mathbb{C}^{\ell_{\text{max}} \times 1}$ and the AWGN added at the mmWave receiver is denoted by $\mathbf{w}^{(m)}[n] \in \mathcal{CN}(0, \sigma_w^2 \mathbf{I}_{M_{\text{Rx}}})$.

III. CHANNEL ESTIMATION METHODS

Due to smaller propagation losses and smaller bandwidth, a sub-6 GHz system has an $\alpha\beta$ times higher SNR compared to the corresponding mmWave system given the same transmit power (see Section II-A). This higher SNR enables us to achieve more accurate channel estimation for the mmWave system with the aid of the sub-6 GHz channel estimate.

We assume that the wavelengths $\lambda^{(s)}$ and $\lambda^{(m)}$, as well as the effective distance \mathbf{D} between the transmitter and receiver are known at the receiver, for example, because they are at known positions. To ensure that the sub-6 GHz channel estimate occupies the bandwidth $B^{(m)}$ of the mmWave system, we first average the $\tilde{\mathbf{H}}^{(s)}[n]$ over subcarriers and use the obtained average value to extrapolate the $\tilde{\mathbf{H}}^{(s)}[n]$ in the frequency

domain. Next, we take the sub-6 GHz channel estimate and rotate its phase by $e^{j2\pi D\xi}$ as follows

$$\begin{aligned}\widehat{\mathbf{H}}^{(s)}[n] &= \widetilde{\mathbf{H}}^{(s)}[n] \odot e^{j2\pi D\xi} \\ &= \sqrt{\eta^{(s)}} \left(A_{\text{fs}}^{(s)} \widetilde{\mathbf{H}}_{\text{fs}}^{(s)}[n] + A_{\text{rp}}^{(s)} \widetilde{\mathbf{H}}_{\text{rp}}^{(s)}[n] \right) \odot e^{j2\pi D\xi} \\ &= \sqrt{\eta^{(s)}} \left(A_{\text{fs}}^{(s)} \underbrace{\widetilde{\mathbf{H}}_{\text{fs}}^{(s)}[n] \odot e^{j2\pi D\xi}}_{\widetilde{\mathbf{H}}_{\text{fs}}^{(m)}[n]} + A_{\text{rp}}^{(s)} \widetilde{\mathbf{H}}_{\text{rp}}^{(s)}[n] \odot e^{j2\pi D\xi} \right) \\ &= \sqrt{\eta^{(s)}} \left(A_{\text{fs}}^{(s)} \widetilde{\mathbf{H}}_{\text{fs}}^{(m)}[n] + A_{\text{rp}}^{(s)} \widetilde{\mathbf{H}}_{\text{rp}}^{(s)}[n] \odot e^{j2\pi D\xi} \right),\end{aligned}\quad (13)$$

where $\xi = \frac{1}{\lambda^{(s)}} - \frac{1}{\lambda^{(m)}}$. Now, the deterministic free-space component of the obtained sub-6 GHz channel estimate $\widehat{\mathbf{H}}^{(s)}[n]$ matches the corresponding one of the mmWave channel estimate $\widetilde{\mathbf{H}}^{(m)}[n]$. Introducing the scaling factors $A_{\text{fs}}^{(s)}$ and $A_{\text{rp}}^{(s)}$, the $\widehat{\mathbf{H}}^{(s)}[n]$ can be rewritten as

$$\begin{aligned}\widehat{\mathbf{H}}^{(s)}[n] &= \sqrt{\eta^{(s)}} \sqrt{\frac{0.1K^{(m)}}{1+0.1K^{(m)}}} \widetilde{\mathbf{H}}_{\text{fs}}^{(m)}[n] \\ &\quad + \sqrt{\eta^{(s)}} \sqrt{\frac{1}{1+0.1K^{(m)}}} \widetilde{\mathbf{H}}_{\text{rp}}^{(s)}[n] \odot e^{j2\pi D\xi}.\end{aligned}\quad (14)$$

As the mmWave K -factor $K^{(m)}$ increases, the amplitude of the stochastic Rayleigh component decreases and the phase of the mmWave channel can be estimated more accurately.

A. Translating

The most straightforward approach to utilize out-of-band information for establishing the mmWave link is only to use the phase-rotated sub-6 GHz channel estimate $\widehat{\mathbf{H}}^{(s)}[n]$, as follows

$$\overline{\mathbf{H}}^{(m)}[n] = \widehat{\mathbf{H}}^{(s)}[n]. \quad (15)$$

In its basic implementation, there is no need for any additional calculations, except the phase rotation in (13). This method performs well for high K -factors, where the stochastic Rayleigh component is negligible. For low K -factors, where the stochastic component dominates the deterministic one, there is no benefit to be gained from using this method.

B. Averaging

To enhance performance for lower K -factors, we propose a method that incorporates the phase-rotated sub-6 GHz channel estimate $\widehat{\mathbf{H}}^{(s)}[n]$ along with the mmWave channel estimate $\widetilde{\mathbf{H}}^{(m)}[n]$. The resulting channel estimate is then given by the average

$$\overline{\mathbf{H}}^{(m)}[n] = \frac{\widehat{\mathbf{H}}^{(s)}[n] + \widetilde{\mathbf{H}}^{(m)}[n]}{2}. \quad (16)$$

At moderate K -factors, this method yields better results on average than the translating method. However, this method involves one more implementation step compared to the translating method. In cases of low and high K -factors, there is still room for improvement by assigning weights different to 0.5 to $\widehat{\mathbf{H}}^{(s)}[n]$ and $\widetilde{\mathbf{H}}^{(m)}[n]$ in (16).

C. Weighting

Performance improvement is achieved through weighting the sub-6 GHz $\widehat{\mathbf{H}}^{(s)}[n]$ and mmWave $\widetilde{\mathbf{H}}^{(m)}[n]$ channel estimates by a weighting factor $W(K^{(m)}, \gamma^{(m)}) \in [0, 1]$ that is a function of the mmWave K -factor $K^{(m)}$ and the mmWave SNR $\gamma^{(m)}$:

$$\begin{aligned}\overline{\mathbf{H}}^{(m)}[n] &= W(K^{(m)}, \gamma^{(m)}) \widehat{\mathbf{H}}^{(s)}[n] \\ &\quad + (1 - W(K^{(m)}, \gamma^{(m)})) \widetilde{\mathbf{H}}^{(m)}[n]\end{aligned}\quad (17)$$

Since the wireless channel is changing, it is important to select an optimum $W(K^{(m)}, \gamma^{(m)})$ for each specific combination of $K^{(m)}$ and $\gamma^{(m)}$. This ensures that the method is optimal for different wireless channel conditions.

During the training phase, we determine and store $W(K^{(m)}, \gamma^{(m)})$ for a set of $K^{(m)}$ and $\gamma^{(m)}$ in a lookup table, see for example Tab. II. To calculate W , we assume perfect knowledge of the mmWave channel $\mathbf{H}^{(m)}[n]$, the $\gamma^{(m)}$ and $K^{(m)}$ by the transmitter and receiver. Next, we find W that results in the minimum mean channel estimation error

$$W(K^{(m)}, \gamma^{(m)}) = \underset{W}{\operatorname{argmin}} E \left\{ W(K^{(m)}, \gamma^{(m)}) \right\}, \quad (18)$$

where the mean channel estimation error is defined by

$$\begin{aligned}E \left\{ W(K^{(m)}, \gamma^{(m)}) \right\} &= \\ &= \frac{1}{LN^{(m)}} \sum_{l=1}^L \sum_{n=1}^{N^{(m)}} \left\| \mathbf{H}_l^{(m)}[n] - \overline{\mathbf{H}}_l^{(m)}[n] \right\|_F^2.\end{aligned}\quad (19)$$

In (19), $\mathbf{H}_l^{(m)}[n]$ denotes the actual channel coefficient and $\overline{\mathbf{H}}_l^{(m)}[n]$ is the estimated channel coefficient for a specific channel realization l . Results are averaged over $L = 1000$ different channel realizations. The lookup table needs to be available at the transmitter and receiver. During data transmission, the previously calculated $W(K^{(m)}, \gamma^{(m)})$ is taken from the lookup table and used to combine sub-6 GHz and mmWave channel estimates.

Compared to the translating method and the averaging method, implementing the weighting method is significantly more demanding. It involves an additional phase for populating the lookup table, and requires the lookup table, $\gamma^{(m)}$ and $K^{(m)}$ to be known at the transmitter and receiver.

IV. SIMULATION-BASED COMPARISON

To evaluate the channel estimation methods proposed, we simulate the achievable SE in a frequency-selective channel. The parameters of the simulation are summarized in Tab. I. For the frequency-selective channel model, we utilize the tapped delay line A (TDL-A) model with the deterministic channel component for the urban macro (UMa) scenario from [22]. Corresponding root-mean-square (RMS) delay spread values for the case without the deterministic channel component are given in Tab. I. The weighting factor lookup table for the TDL-A channel model is given in Tab. II.

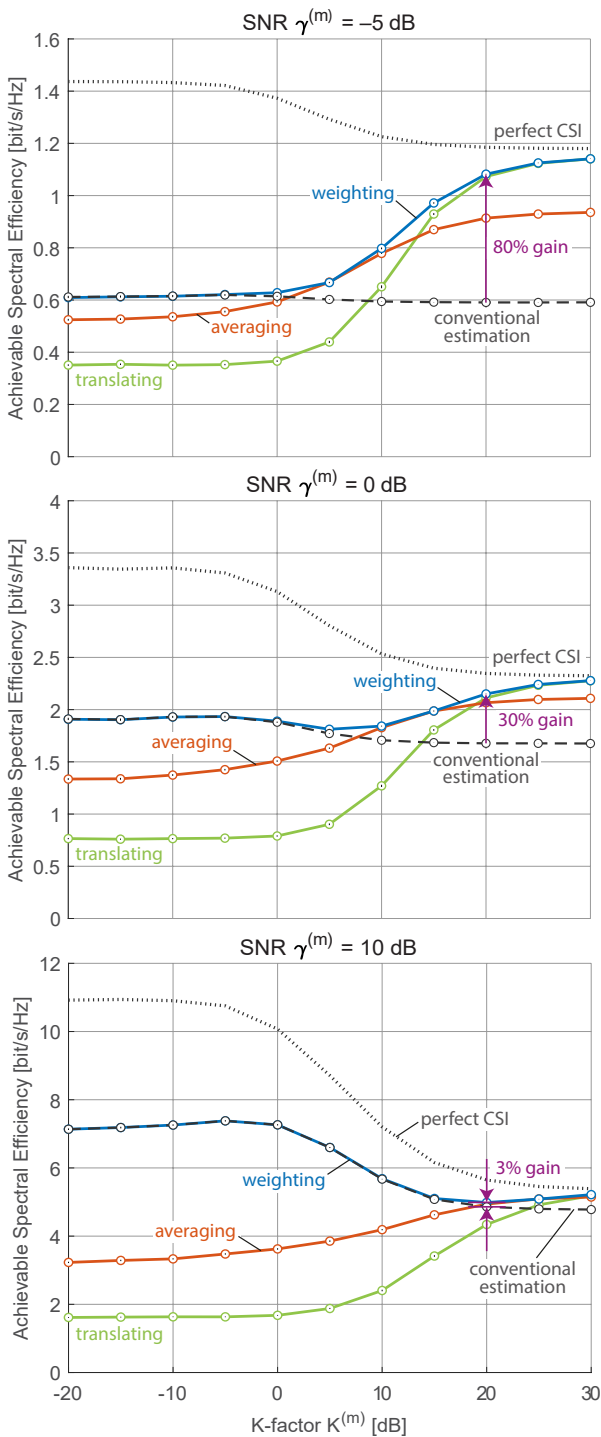


Fig. 3. For the TDL-A 4×4 MIMO channel, the proposed weighting method achieves up to 80% higher SE. The small vertical bars within the circular markers indicate the 95% confidence intervals.

We consider the achievable SE (achievable rate per bandwidth) as the main performance metric for MIMO systems. Since SE is rate per bandwidth, this metric does not depend on the employed transmission bandwidth and therefore facilitates direct comparison of results. The achievable SE in bits/s/Hz

TABLE I
SIMULATION PARAMETERS

Parameter	Value	
Frequency Band	sub-6 GHz	mmWave
Carrier Frequency f_c [GHz]	2.55	25.5
Wavelength λ [cm]	11.76	1.176
Bandwidth B [MHz]	10.08	100.8
Subcarrier Spacing Δf [kHz]	60	60
Cyclic Prefix t_{CP} [μ s]	1.19	1.19
Noise Figure F [dB]	3	3
Antenna Spacing [cm]	0.05λ	0.5λ
Channel Model	TDL-A 1148 ns	TDL-A 841 ns

averaged over $N^{(m)}$ subcarriers is given by

$$SE = \frac{1}{N^{(m)}} \sum_{n=1}^{N^{(m)}} \log_2(1 + \text{SINR}[n]) \quad (20)$$

with

$$\text{SINR}[n] = \frac{\sum_{\mu=1}^{\ell_{\max}} \sum_{\nu=\mu}^{\ell_{\max}} |\overline{G}_{\mu,\nu}^{(m)}[n]|^2}{\sum_{\mu=1}^{\ell_{\max}} \sum_{\substack{\nu=1 \\ \nu \neq \mu}}^{\ell_{\max}} |\overline{G}_{\mu,\nu}^{(m)}[n]|^2 + \sigma_w^2 \|\overline{\mathbf{Q}}^{(m)}[n]\|_F^2}. \quad (21)$$

In (21), $\overline{G}_{\mu,\nu}^{(m)}[n]$ with $\mu, \nu \in \{1, \dots, \ell_{\max}\}$ represent entries of the channel gain matrix $\mathbf{G}^{(m)}[n] \in \mathbb{C}^{\ell_{\max} \times \ell_{\max}}$ for n -th subcarrier which is given by

$$\overline{\mathbf{G}}^{(m)}[n] = \left(\overline{\mathbf{Q}}^{(m)}[n] \right)^H \mathbf{H}^{(m)}[n] \left(\mathbf{P}^{(m)} \right)^{1/2} \overline{\mathbf{F}}^{(m)}[n]. \quad (22)$$

After averaging over $L = 1000$ different channel realizations, we obtain the simulation results shown in Fig. 3. As a conventional channel estimation method, we use the achievable SE for the case that only the mmWave channel estimate $\overline{\mathbf{H}}^{(m)}[n] = \tilde{\mathbf{H}}^{(m)}[n]$ is employed. The achievable SE for the case of perfect CSI ($\overline{\mathbf{H}}^{(m)}[n] = \mathbf{H}^{(m)}[n]$) is shown in Fig. 3 as well.

Results at SNR of -5 dB: When the translating method is used at a high K -factor $K^{(m)}$, it leads to 80% improvement in achievable SE as compared to the case when estimating using only the mmWave band. However, the performance of the translating method is poor at low K -factor. The averaging method yields better results at low K -factor. At high K -factor, the averaging method performs worse than the translating method. Ultimately, the weighting method is for all K -factors at least as good or better than the translating method and the averaging method.

Results at SNR of 0 dB: Again, the weighting method outperforms the translating method and the averaging method, although the gain compared to conventional channel estimation at high K -factors is less (30%).

Results at SNR of 10 dB: The gain compared to conventional channel estimation at high K -factors is now only 3%. Therefore, it is questionable if the effort justifies the gain.

TABLE II
WEIGHTING FACTOR W LOOKUP TABLE
TDL-A CHANNEL

$K^{(m)}$ [dB]	$\gamma^{(m)}$ [dB]							
	-15	-10	-5	0	5	10	15	20
-20	0.83	0.92	0.98	1	1	1	1	1
-15	0.81	0.91	0.97	0.99	1	1	1	1
-10	0.76	0.86	0.95	0.99	1	1	1	1
-5	0.63	0.75	0.89	0.97	1	1	1	1
0	0.4	0.55	0.76	0.89	0.99	1	1	1
5	0.19	0.33	0.56	0.79	0.93	1	1	1
10	0.1	0.18	0.35	0.61	0.85	0.99	1	1
15	0.04	0.1	0.19	0.39	0.66	0.87	0.99	1
20	0.01	0.03	0.1	0.2	0.41	0.68	0.87	0.99
25	0	0	0.02	0.1	0.2	0.41	0.68	0.87
30	0	0	0	0.02	0.1	0.2	0.41	0.68

Note that for high $K^{(m)}$, W is close to 1, as the phase-rotated sub-6 GHz estimate significantly improves channel estimation. Conversely, for low $K^{(m)}$, the phase-rotated sub-6 GHz estimate does not play a significant role. In this case, W is close to 0.

V. CONCLUSION

In this paper, we propose three novel channel estimation methods for mmWave MIMO systems based on using sub-6 GHz out-of-band information. The SNR and K -factor affect the performance of the proposed channel estimation methods to a great extent. The proposed methods lead to a significant increase in the achievable SE in the low-SNR regime, while the gains are negligible in the high-SNR regime. The translating method performs well at high K -factors. The averaging method performs well at moderate K -factor. The weighting method is better (high K -factor) or at least as good (low K -factor) as the conventional channel estimation method using only the mmWave band.

ACKNOWLEDGMENT

This work was supported by the Austrian Research Promotion Agency (FFG) via the research project Intelligent Intersection (ICT of the Future, Grant 880830). The work of M. Hofer and T. Zemen was supported by the principal scientist grant DEDICATE. The work of M. Mussbah was supported by the Christian Doppler Research Association.

REFERENCES

- [1] B. Ai, A. F. Molisch, M. Rupp, and Z. D. Zhong, "5G Key Technologies for Smart Railways," *Proceedings of the IEEE*, vol. 108, no. 6, 2020.
- [2] R. W. Heath, N. González-Prelcic, S. Rangan, W. Roh, and A. M. Sayeed, "An Overview of Signal Processing Techniques for Millimeter Wave MIMO Systems," *IEEE Journal of Selected Topics in Signal Processing*, vol. 10, no. 3, pp. 436–453, 2016.
- [3] T. S. Rappaport, S. Sun, R. Mayzus, H. Zhao, Y. Azar, K. Wang, G. N. Wong, J. K. Schulz, M. Samimi, and F. Gutierrez, "Millimeter Wave Mobile Communications for 5G Cellular: It Will Work!" *IEEE Access*, vol. 1, pp. 335–349, 2013.
- [4] N. Gonzalez-Prelcic, A. Ali, V. Va, and R. W. Heath, "Millimeter-Wave Communication with Out-of-Band Information," *IEEE Communications Magazine*, vol. 55, no. 12, pp. 140–146, 2017.
- [5] M. Hofer, D. Löschenbrand, J. Blumenstein, H. Groll, S. Zelenbaba, B. Rainer, L. Bernadó, J. Vychodil, T. Mikulasek, E. Zöchmann, S. Sangodoyin, H. Hammoud, B. Schrenk, R. Langwieser, S. Pratschner, A. Prokes, A. F. Molisch, C. F. Mecklenbräuker, and T. Zemen, "Wireless Vehicular Multiband Measurements in Centimeterwave and Millimeterwave Bands," in *2021 IEEE 32nd Annual International Symposium on Personal, Indoor and Mobile Radio Communications (PIMRC)*, 2021, pp. 836–841.
- [6] M. Hofer, D. Löschenbrand, S. Zelenbaba, A. Dakić, B. Rainer, and T. Zemen, "Wireless 3GHz and 30 GHz Vehicle-to-Vehicle Measurements in an Urban Street Scenario," in *2022 IEEE 96th Vehicular Technology Conference (VTC2022-Fall)*, 2022.
- [7] D. Dupleich, R. Müller, M. Landmann, E.-A. Shinwasusin, K. Saito, J.-I. Takada, J. Luo, R. Thomä, and G. Del Galdo, "Multi-Band Propagation and Radio Channel Characterization in Street Canyon Scenarios for 5G and Beyond," *IEEE Access*, vol. 7, pp. 160 385–160 396, 2019.
- [8] F. Pasic, D. Schützenhöfer, E. Jirousek, R. Langwieser, H. Groll, S. Pratschner, S. Caban, S. Schwarz, and M. Rupp, "Comparison of Sub 6 GHz and mmWave Wireless Channel Measurements at High Speeds," in *16th European Conference on Antennas and Propagation (EuCAP 2022)*, 2022.
- [9] F. Pasic, M. Hofer, M. Mussbah, H. Groll, T. Zemen, S. Schwarz, and C. F. Mecklenbräuker, "Statistical Evaluation of Delay and Doppler Spreads in sub-6 GHz and mmWave Vehicular Channels," in *2023 IEEE 97th Vehicular Technology Conference (VTC2023-Spring)*, 2023.
- [10] F. Pasic, N. Di Cicco, M. Skocaj, M. Tornatore, S. Schwarz, C. F. Mecklenbräuker, and V. Degli-Esposti, "Multi-Band Measurements for Deep Learning-Based Dynamic Channel Prediction and Simulation," *IEEE Communications Magazine*, vol. 61, no. 9, pp. 98–104, 2023.
- [11] Y. Kishiyama, A. Benjebbour, T. Nakamura, and H. Ishii, "Future steps of LTE-A: evolution toward integration of local area and wide area systems," *IEEE Wireless Communications*, vol. 20, no. 1, pp. 12–18, 2013.
- [12] A. Ali, N. González-Prelcic, and R. W. Heath, "Millimeter Wave Beam-Selection Using Out-of-Band Spatial Information," *IEEE Transactions on Wireless Communications*, vol. 17, no. 2, pp. 1038–1052, 2018.
- [13] —, "Estimating millimeter wave channels using out-of-band measurements," in *2016 Information Theory and Applications Workshop (ITA)*, 2016.
- [14] P. Kyösti, P. Zhang, A. Pärssinen, K. Haneda, P. Koivumäki, and W. Fan, "On the Feasibility of Out-of-Band Spatial Channel Information for Millimeter-Wave Beam Search," *IEEE Transactions on Antennas and Propagation*, vol. 71, no. 5, pp. 4433–4443, 2023.
- [15] M. S. Sim, Y.-G. Lim, S. H. Park, L. Dai, and C.-B. Chae, "Deep Learning-Based mmWave Beam Selection for 5G NR/6G With Sub-6 GHz Channel Information: Algorithms and Prototype Validation," *IEEE Access*, vol. 8, pp. 51 634–51 646, 2020.
- [16] K. Ma, S. Du, H. Zou, W. Tian, Z. Wang, and S. Chen, "Deep Learning Assisted mmWave Beam Prediction for Heterogeneous Networks: A Dual-Band Fusion Approach," *IEEE Transactions on Communications*, vol. 71, no. 1, pp. 115–130, 2023.
- [17] B. Getu and J. Andersen, "The MIMO cube - a compact MIMO antenna," *IEEE Transactions on Wireless Communications*, vol. 4, no. 3, pp. 1136–1141, 2005.
- [18] R. Ghods, A. Gallyas-Sanhueza, S. H. Mirfarshbafan, and C. Studer, "BEACHES: Beamspace Channel Estimation for Multi-Antenna mmWave Systems and Beyond," in *2019 IEEE 20th International Workshop on Signal Processing Advances in Wireless Communications (SPAWC)*, 2019.
- [19] L. Cimini, "Analysis and Simulation of a Digital Mobile Channel Using Orthogonal Frequency Division Multiplexing," *IEEE Transactions on Communications*, vol. 33, no. 7, pp. 665–675, 1985.
- [20] S. Schwarz, M. Wrulich, and M. Rupp, "Mutual information based calculation of the Precoding Matrix Indicator for 3GPP UMTS/LTE," in *2010 International ITG Workshop on Smart Antennas (WSA)*, 2010, pp. 52–58.
- [21] H. Miao, J. Zhang, P. Tang, L. Tian, X. Zhao, B. Guo, and G. Liu, "Sub-6 GHz to mmWave for 5G-Advanced and Beyond: Channel Measurements, Characteristics and Impact on System Performance," *IEEE Journal on Selected Areas in Communications*, vol. 41, no. 6, pp. 1945–1960, 2023.
- [22] 3GPP, "Study on channel model for frequencies from 0.5 to 100 GHz," 3rd Generation Partnership Project (3GPP), Technical report (TR) 38.901, 2022, version 17.0.0.